A Review of Porous Manganese Oxide Materials

Stephanie L. Brock,[†] Niangao Duan,[‡] Zheng Rong Tian,[†] Oscar Giraldo,[†] Hua Zhou,[†] and Steven L. Suib*[,†,‡,§]

U-60, Department of Chemistry, Institute of Materials Science, and Department of Chemical Engineering, University of Connecticut, Storrs, Connecticut 06269-4060

Received April 1, 1998. Revised Manuscript Received July 1, 1998

This review concerns the synthesis, characterization, and applications of porous manganese oxides during the last two years. The synthesis of porous tunnel structures, layered structures, and related materials is discussed. Both microporous and mesoporous systems materials are covered here. Characterization discussed here focuses around structural studies. The focus of the application sections include electrochemical and catalytic studies.

Contents

Strategies for the Preparation of Novel Manganese Oxides

Micro- and mesoporous manganese oxides, as well as layered claylike manganese oxide materials are prepared via a variety of routes. Many of the materials with similar gross structural features nevertheless show a diversity of properties depending on the specific synthetic route. These differences can be attributed to variations in particle size and the type and amount of defects in the structures. For this reason, small changes in synthetic parameters can result in materials with novel catalytic, electrochemical, and ion-exchange properties. Because these porous manganese oxide materials are metastable (in contrast to nonporous perovskite manganese oxides), the majority of synthetic preparations fall in the chimie douce regime. The emphasis of this review will be on recent preparations based on novel and revisited synthetic techniques, including precipitation/ion-exchange/hydrothermal routes, microwave heating, sol−gel, and high-temperature solid-state routes.

A. Precipitation, Ion-Exchange, and Hydrothermal Routes. Precipitation routes involving redox reactions of Mn^{7+} (permanganate) and/or Mn^{2+} salts are common for formation of manganese oxides because molecular Mn^{4+} materials suitable for precursors are rare. Typical materials formed from precipitation routes include layered manganese oxides (birnessites) and condensed phase materials such as hausmannite (Mn_3O_4). The birnessites incorporate cations (typically alkali or alkaline earth metal ions) between the layers to balance the negative charge on the sheets, as well as differing amounts of hydrated water. They can undergo ion-exchange reactions, replacing the cations between the layers with other alkali or alkaline earth metal ions as well as protons. Hydrothermal treatment of birnessites can lead to a variety of porous structures with tunnels ranging from 1 × 1 (pyrolusite) to 2 × 4 (RUB-7) and 3 × 3 (todorokite).

Recently, Luo et al.[1] performed a detailed investigation on the contribution of various synthetic parameters to the crystallinity and ion-exchange properties of resulting birnessites. The following synthetic route they investigated was developed for the preparation of todorokites with increased thermal stability[2]

$$MnX + 0.2MgX + xsNaOH \rightarrow Mn(OH)_2 + 0.2Mg(OH)_2 + NaX \quad (1)$$

$$Mn(OH)_2 + 0.2Mg(OH)_2 + NaX + KMnO_4 \rightarrow Na_4(Mn,Mg)_{14}O_{27}\cdot 21H_2O \quad (2)$$

The mixed solution of manganese and magnesium salts (chloride, acetate, nitrate, sulfate) is added to the cooled sodium hydroxide solution with stirring to form the magnesium/manganese hydroxide mixture. Potassium permanganate solution is added subsequently, forming a dark suspension. The parameters investigated include basicity, temperature, effect of the anion (X = acetate, chloride, nitrate, sulfate), effect of the MnO_4^-/Mn^{2+} ratio and the effect of Mg^{2+}. The crystallinity of the materials was evaluated by X-ray diffraction (XRD).

Generally, the synthesis of sodium birnessite is characterized by an induction period, a fast crystallization period, and a slow crystallization period. The length of each of these periods has a strong dependence on temperature, with increasing temperature in the range −2 to 85 °C resulting in decreased time for crystallization. Initial products include an unidentified material referred to as prephase I (related to hausman-

* To whom correspondence should be addressed.
[†] U-60, Department of Chemistry.
[‡] Institute of Materials Science.
[§] Department of Chemical Engineering.

10.1021/cm980227h CCC: $15.00
Published on Web 09/18/1998

nite, γ-Mn_3O_4), the layered manganese oxide-hydroxide, feitknechtite, and Na birnessite. In time, prephase I and feitknechtite are converted to birnessite. The completion of this transformation can take up to 45 days at room temperature versus <1 day at 85 °C. Heating of the materials results in a decreased tendency toward cation exchange: at 65 °C, only partial exchange of Mg^{2+} for Na^+ is achieved.

Increased basicity has a similar, though less pronounced, effect as that of increased temperature. As basicity is increased, the induction time is decreased, the crystallization rate is increased, and the materials are more difficult to ion exchange. Basicities of >10 are required to form birnessite. The mechanism of formation of birnessite is believed to involve solubilization of MnO_x units in base, which subsequently knit together to form layers. In such a mechanism, the observed layered oxide−hydroxide phase, feitknechtite, is a reasonable intermediate. Thus, increasing basicity leads to increased solubility and increases in crystal growth and size. Likewise, increasing temperature also increases solubility of precursors leading to accelerated crystal growth.

Because the average oxidation state of manganese in the birnessite product is typically between 3.4 and 3.99, it stands to reason that the Mn^{7+}/Mn^{2+} ratio in the initial mixture would have a profound effect on the product distribution and crystallinity. Luo and Suib[1] investigated Mn^{7+}/Mn^{2+} ratios in the range 0.17−0.72. In the range 0.17−0.24, the main products are lower valent: for examples, hausmannite (γ-Mn_3O_4) and feitknechtite [β-MnO(OH)]. From 0.24 to 0.32, the proportion of birnessite and feitknechtite increase to a maximum. Above 0.32, the induction period increases and the crystallinity decreases until the products are almost amorphous (>0.56).

The role of Mg^{2+} in the synthesis has been the subject of some interest. Mg^{2+} incorporated into the beginning of the birnessite synthesis will yield todorokite materials with increased thermal stability, but the role of the Mg^{2+} remains a mystery. Mg^{2+}/Mn^{2+} ratios of 0 and 0.2 were investigated. Without Mg, the crystallization rate is almost 5 times greater than when Mg is present and it is likely that formation of less soluble $Mg(OH)_2$ particles may act to impede nucleation of birnessite. However, the Mg sample holds physisorbed and interlayer water more strongly [as evidenced by differential scanning calorimetry (DSC)], which is a function of the higher ionic strength of Mg. Partial oxidation of dried samples in air leads to the formation of low valent feitknechtite and hausmannite for the Mg-free sample versus birnessite for the Mg-incorporated sample, suggesting that Mg facilitates oxidation of manganese hydroxide to yield birnessite. Furthermore, long aging times result in formation of manganite [γ-MnO(OH)] in the Mg-free sample, so, in addition to facilitating the formation of birnessite, Mg also acts to stabilize the resulting product. This facilitation, however, is not true in acid solutions. Mg-free birnessite forms a stable H-birnessite, whereas the Mg-incorporated sample dissolves, which is not a surprising result because Mg−O bonds are easily broken by H^+.

Finally, anion effects in the precursor Mn^{2+} and Mg^{2+} salts were investigated for acetate, chloride, nitrate, and sulfate. The products obtained from all of the anions have identical properties and no evidence of the anion being incorporated into the product was found. The crystallization rates do seem to vary somewhat, with acetate being the fastest. This result may be attributed to the fact that acetate has the highest basicity of the anions investigated because the influence of base on the synthesis is demonstrated to be very important.

From the parameters investigated, the authors[1] conclude that formation of birnessites with high crystallinity and good ion-exchange properties can be obtained for hydroxide concentrations >2.6 M, a Mn^{7+}/Mn^{2+} ratio of 0.32, and temperatures approaching, but not exceeding, 65 °C. Depending on the properties desired, Mg can be incorporated into the synthesis as well.

Feng and co-workers[3−5] have recently reported the synthesis of Na[3] and Li[4] birnessites using hydrogen peroxide as an oxidant for Mn^{2+} salts in basic solutions. Oxidation of Mn^{2+} salts is a common route to birnessites, with the most typical oxidant being oxygen itself. The authors reacted $Mn(NO_3)_2$ salt solution with a mixed solution of Na, Li, or K hydroxide and hydrogen peroxide while rapidly stirring at room temperature. The formation and subsequent oxidation of $Mn(OH)_2$ led to formation of birnessite.

For the sodium birnessite, the authors tried varying the concentration of $NaOH/Mn(NO_3)_2$ ratio and obtained results similar to those just outlined by Luo and Suib.[1] An optimum ratio of 4.0 was found. Increasing the ratio resulted in amorphous material and decreasing the ratio caused preferential formation of feitknechtite. The Li material showed a similar dependence on OH^-/Mn^{2+} concentration with an optimum ratio of 3.5 to 3.7. Both the Na and Li materials can undergo facile ion exchange with a variety of alkali cations (Li → K), but the Li material can only be ~80% exchanged with Mg^{2+}.

The transformation of sodium birnessite prepared in this way to tunnel structures has also been investigated and the results are the same as those obtained for birnessites prepared via other routes. Hydrothermal treatment was performed at 150 °C for 2 days under autogenous pressure on the Na material,[3] as well as materials obtained by ion-exchange with Li, K, and Mg.[5] A dependence of the product on the ion size and the basicity of the hydrothermal solution is observed. Treatment of Li, Na, and K birnessites in chloride salts (neutral pH) yields birnessites with reduced crystallinity relative to the starting materials. For Mg^{2+}, the expected 3 × 3 todorokite phase is obtained. As expected, increasing the basicity increases the crystallinity of Na and K, whereas Li birnessite transforms to the more stable spinel structure. In acidic solution, Na (HCl) and Mg (H_2SO_4) both transform to the 1 × 1 pyrolusite material, K (H_2SO_4) forms the 2 × 2 hollandite, and Li (H_2SO_4) the 1 × 2 ramsdellite structure. Thus, structural transformations from birnessite appear to occur more readily in neutral to acidic solutions, with the exception of Li-birnessite, and the resulting products show some dependence on the identity of the cation. This dependence on template ion is clearly the case for OMS-1 materials[2] and for RUB-7, as discussed later.[6]

The formation of structures up to the 3 × 3 todorokite has been established for quite some time, however, stabilization of larger pore sizes and asymmetric tunnel

structures has remained a synthetic challenge. Recently, Rziha, Gies, and Rius have reported a new manganese oxide structure with a 2 × 4 tunnel (RUB-7) containing Rb^+ cations in the tunnels as well as an unknown, but presumably layered phase (RUB-8).[6] The material was prepared via hydrothermal treatment of Rb birnessite with Rb(OH) in a gold ampule at 350 °C and 2 kBar of pressure for 2 days. This phase is not unique to Rb. Experiments were done starting from Rb, Na, and K birnessites, all prepared via a modified Stohli method (treatment of basic Mn^{2+} with oxygen) and RbOH, NaOH, KOH. In fact, Na appears to be a stronger director to this structure type, as materials with Na, Na−K, and Na−Rb all resulted in preferential formation of RUB-7. Potassium, when not in the presence of sodium, directs preferentially toward the 2 × 2 cryptomelane (hollandite) structure. Despite the relatively high temperature at which the material is prepared, the RUB-7 phase is poorly crystalline and hausmannite is frequently present as an impurity. Thus, high-temperature and high-pressure hydrothermal routes may find new materials by examining a new section of the phase diagram and ease their identification by preparation of larger crystals. However, the synthetic requirements are not suitable for the preparation of large-scale materials and thus the bulk properties of RUB-7 remain uninvestigated.

B. Sol−Gel Routes. In addition to routes that proceed by oxidation of Mn^{2+} salts with $KMnO_4$, O_2, H_2O_2, etc., it is possible to synthesis microporous and layered manganese oxides by reduction of $KMnO_4$ with organic reducing agents. Such routes frequently result in formation of a sol or gel. Although the initial report of manganese oxide jellies was made over 80 years ago,[7] it was not until 1990 that such routes were re-examined for formation of microporous manganese oxides.[8−10] Very recently, Ching and co-workers have investigated the synthesis of the 2 × 2 material, cryptomelane (hollandite) and birnessite, by sol-gel routes.[11,12]

Two different groups of organic species have been investigated as reducing agents: multifunctional carboxylic acids, such as fumaric and maleic acids,[11] and polyols, including sugars.[12] The authors have investigated the effects of cations (Na, K), ratio of reducing agent to permanganate, temperature of calcination, and effect of pH on the structure of the materials produced, along with their ion-exchange properties.

The preparation with polyols, using glucose as an example, is carried out starting from aqueous $KMnO_4$ and glucose solutions, which are stirred quickly together, and then let stand to gel (30 s). A dark monolithic gel is obtained and dried overnight at 110 °C, occasionally pouring off water liberated during gel syneresis. The subsequent material is calcined at 400 °C for 2 h, ground, washed with water to remove surface adhered K ions, and dried at 110 °C overnight. The structure of the resulting material depends on synthetic parameters, as illustrated in Scheme 1. For high concentrations of reactants (0.27 M $KMnO_4$, glucose:MnO_4^- ratio = 1.5), a monolithic gel yielding K birnessite is obtained, whereas lower concentrations produce a flocculant gel, yielding the 2 × 2 cryptomelane and or Mn_2O_3 (bixbyite). Similarly, if the glucose:MnO_4^- ratio is decreased to 0.37, a flocculant gel results, with

Scheme 1

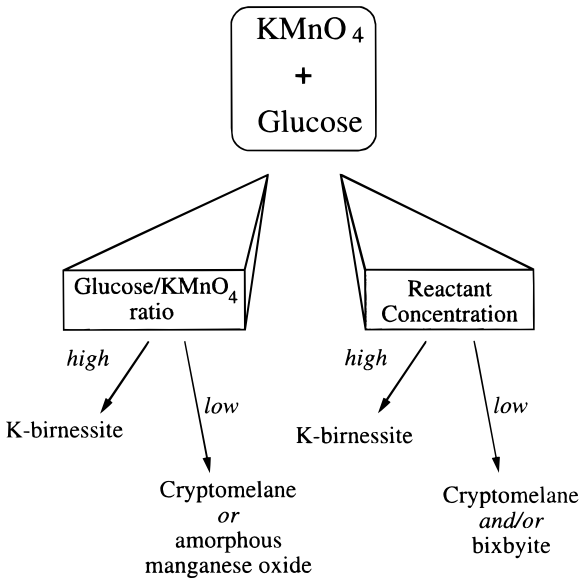

cryptomelane as a product. Further decreasing the ratio to 0.2 results in an amorphous manganese oxide. The shift in structure from birnessite to cryptomelane is a function of the different average oxidation states of manganese in the products (3.63 and 3.88, respectively), which is mirrored by the K:Mn ratios found in the two materials (0.28 and 0.125, respectively). Lower glucose:MnO_4^- ratios result in the higher oxidation state cryptomelane material. Decreases in amounts of glucose either by decreasing the overall concentration of reagents or varying the ratio also result in more flocculant gels, as there is not enough of the organic cross-linking agent to form a monolith. Such dispersed gels are likely to lose K^+ to the mother liquor, again resulting in a preference to the cryptomelane structure. Similarly, too much glucose results in reduction all the way to Mn_2O_3.

In contrast to the potassium system, gels produced with $NaMnO_4$ are less responsive to the glucose:MnO_4^- ratio, and no 2 × 2 cryptomelane-type products are obtained. This result is not surprising because the K^+ cation is of the ideal dimension to fit in the 2 × 2 tunnels and manganese oxide syntheses involving K^+ often lead to this structure, whereas the Na^+ cation is on the small side to stabilize the 2 × 2. Two different layered products are formed for Na^+, one of which is dehydrated, yielding an interlayer distance of 5.5 Å. The dehydrated phase is obtained from calcining at 800 °C, and this phase can be transformed into the hydrate by stirring in water. Another difference between the potassium and sodium systems is their thermal stabilities. Thermal treatment of the 7 Å hydrated Na birnessite leads to Mn_3O_4 at 600 °C, the K birnessite produces cryptomelane, and Mn_3O_4 is not produced until 800 °C.

The reaction of $KMnO_4$ with fumaric or maleic acids proceeds by introduction of solid fumaric or maleic acid to a stirred solution of $KMnO_4$-to-acid of 3:1, resulting in a flocculant brown-black gel. The gel is washed, dried at 110 °C, and calcined at 450 °C for 2 h. Subsequent washing of the calcined material with dilute HCl and water removes surface adsorbed potassium ions. Similar to the results obtained with sugars and poly-ols, high

concentrations of reagents lead to K birnessite and very dilute solutions yield Mn_2O_3. Although the permanganate salts of Li^+, Na^+, Mg^{2+}, and Ca^{2+} were all investigated, only Ca^{2+} yielded a pure hollandite material.

These sol−gel routes introduce some flexibility into the processability of manganese oxide materials, and the products have unique properties not found from materials produced by the more traditional precipitation/hydrothermal routes. The morphologies of sol−gel materials are more particulate in appearance, in contrast to the commonly observed plates (birnessite) and needles (cryptomelane). Additionally, the alkali cations appear to be tightly bound in these materials and will exchange only partially with other alkali, alkaline earth, or ammonium cations.

The sol−gel synthesis of the 2 × 2 material cryptomelane (hollandite) using microwave heating for the calcination stages has also been investigated.[13] Microwave heating has been proven to be an effective technique for fast and selective synthesis of zeolitic materials.[14] Given the large dielectric constant of MnO_2, it is likely that the influence of microwave irradiation will have a pronounced effect on the synthesis of porous manganese oxides. The manganese oxide gel was prepared from $KMnO_4$ and maleic acid in a manner similar to that already outlined. Using a microwave oven as the heating source, the formation of cryptomelane begins at 320 °C, much lower than the 390 °C required by conventional heating sources. Additionally, the crystallization appears to be much faster in the microwave preparation as sharp peaks corresponding to cryptomelane appear after just 10 min at 425 °C. After 20 min of conventional heating, cryptomelane is still poorly crystalline, requiring several hours of calcination to form a well-crystallized sample. Finally, under microwave heating conditions, the phase transformation to bixbyite appears to be more facile, occurring at temperatures as low as 425 °C within 3 h of time, relative to > 650 °C necessary for conventional heating. The reported formation of bixbyite (Mn_2O_3) rather than hausmannite (Mn_3O_4) as reported from sol−gel studies of Ching et al.,[9,11,12] may be due to slight differences in the synthetic procedures.

C. High-Temperature Solid-State Routes. Microporous materials are most commonly produced by soft-chemistry routes as porous materials are generally more stable at lower temperature. Additionally, such routes afford materials with smaller crystallite sizes, which may be more desirable for ion-exchange and catalytic properties. Nevertheless, high-temperature routes can result in the formation of structurally porous phases. Recently, Raveau and co-workers reported the synthesis of a new manganite $Ba_6Mn_{24}O_{48}$ with a composite tunnel structure consisting of units of hollandite (2 × 2) linked to pyrolusite (1 × 1) with Ba^{2+} cations in the hollandite tunnels.[15] The space group of this material is $I4/m$ with a = 18.173(2) Å and c = 2.836(1) Å. The material was prepared from grinding together $BaCO_3$ and MnO_3 with Bi_2O_3 incorporated as a melting agent. The mixture was heated in air to 900 °C over 3 h and maintained at this temperature for 20 h. The temperature was further increased to 1200−1279 °C (300 °C/h) for 2 h and cooled at a rate of 1 °C/h. Such a material was found to be highly ordered, relative to chimie douce preparations of other tunnel structures. Because of the high temperature used in the synthesis, no H_2O is incorporated. Nevertheless, the synthesis requires optimization because the $Ba_6Mn_{24}O_{48}$ material is produced along with a number of other manganate phases such as $BaMnO_3$. A pure polycrystalline phase of $Ba_6Mn_{24}O_{48}$ is formed from BaO_2 and Mn_2O_3.

Scheme 2. Tunnel Sizes of Various OMS and OL Materials

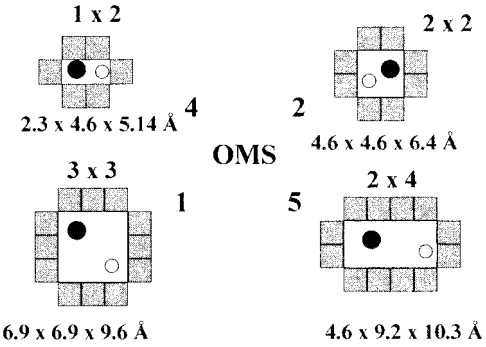

Structural Studies

This section reviews structural work on manganese oxides with tunnel and layer structures. We focus on recent progress in relation to molecular sieve science and catalysis. For layered manganese oxides as magnetoresistance materials, readers are referred to a review by Rao, Cheetham, and Mashesh.[16] Note that the lattice parameters and space groups for these materials can be found in original references. A brief summary is given next.

A. Tunnel Structures. Mixed valent manganese oxides with a general formula A_xMnO_2 often crystallize as microporous tunnel structures. The building block is MnO_6 octahedra. These octahedra share their corners or edges to form chainlike slabs and further cross-link to build one-dimensional (1D) tunnels. Cations reside in these pores to support the framework and to maintain charge balance.

Structures of porous manganese oxides can be described as a combination of P and B building blocks: P (pyrolusite), and B (birnessite), where P represents corner-sharing and B the edge-sharing mode of the octahedral building blocks. The size and shape of tunnels known to date include ramsdellite (2 × 1), hollandite (2 × 2), romanechite (2 × 3), todorokite (3 × 3), and synthetic $Rb_{27}MnO_2$ (2 × 5). In addition, transmission electron microscopy (TEM) studies have revealed many composite structures consisting of different tunnel sizes in natural minerals.

Two new members of this family materials have been recently synthesized.[6,15] One is the alkaline manganese oxide with 2 × 4 tunnels, designated RUB-7;[6] another is a composite structure of hollandite and pyrolusite, showing 2 × 2 and 2 × 3 micropores.[15] The RUB-7 materials is believed to be a monoclinic $C2/m$ system with a = 14.191(3) Å, b = 2.851(1) Å, c = 24.343(7) Å, and β = 91.29°. A $Na_{0.44}MnO_2$ structure is also described in this section.[17] Tunnel structures of many of the OMS and OL materials are given in Scheme 2. Note that these are square tunnels and that the diagonal distances across the opposite sides of the tunnels are

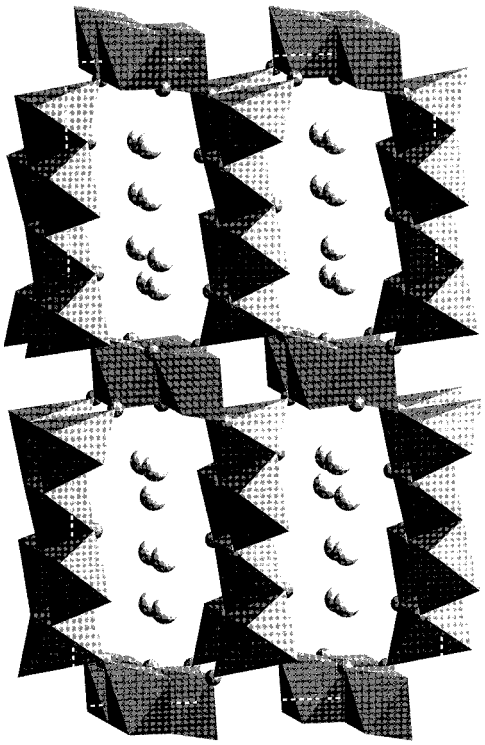

Figure 1. Structure of RUB-7.

significantly larger than the tunnel edge size. Water molecules (black filled circles) and cations (grey filled circles) are present in the tunnels. This is reflected in the pore size distributions of these materials as discussed under the subsection Porosity.

(1) RUB-7. This structure consists of MnO_6 octahedra that form 2 × 4 channels.[6] The Rb^+ ions are located within the channels and distributed along the *b*-axis with disorder. Different Mn−O bond lengths are found for different manganese sites, which is evident from the distortion of the octahedra as illustrated in Figure 1. This structure was solved with a combination of single-crystal XRD and Rietveld analyses. Weissenberg photographs were used to obtain approximate cell parameters and to determine the space group. The Rietveld refinement converged with a residue factor R_{wp} of 18%. Difficulties in determining this structure include preferred orientation of the needlelike morphologies, anisotropic broadening, and thermal motion of Rb ions in the tunnels.

(2) $Ba_6Mn_{24}O_{48}$. This is a composite tunnel structure of hollandite and rutile.[16] In this structure, two types of columns share the edges of their octahedra to generate a 10-sided tunnel and a 2 × 2 tunnel. This structure is shown in Figure 2. Electron diffraction and high resolution transmission electron microscopy (HRTEM) data clearly show this phase is a composite structure, built up of two tetragonal body centered sublattices with a = 18.2 Å, c_1 = 2.8 Å, and c_2 = 4.6 Å. The HRTEM data suggest that the octahedral $[Mn_4O_8]$ framework is made of hollandite and rutile columns. Rietveld refinement studies confirmed the composite structure.

(3) $Li_{0.44}MnO_2$. This is a similar structure as that of $Na_{0.44}MnO_2$.[17] The structure can be viewed as an Mn−O framework consisting of MnO_6 octahedra and MnO_5 square pyramids, as shown in Figure 3. The space group is *Pbam* with a = 8.9316(2) Å, b = 24.4350(5) Å, and c = 2.6307(2) Å. This structure exhibits two types of tunnels. The smaller pores are defined by four MnO_6 octahedra and two MnO_5 square pyramids. The larger pores are defined by 10 MnO_6 octahedra and two MnO_5 square pyramids. Rietveld analyses of neutron diffraction data were carried out to refine the structures. Distinct Li sites are found to reside within these 1D tunnels.

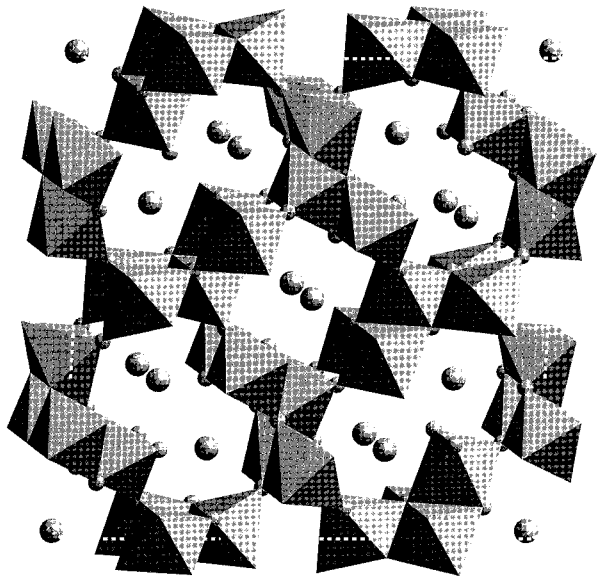

Figure 2. Structure of $Ba_6Mn_{24}O_{48}$.

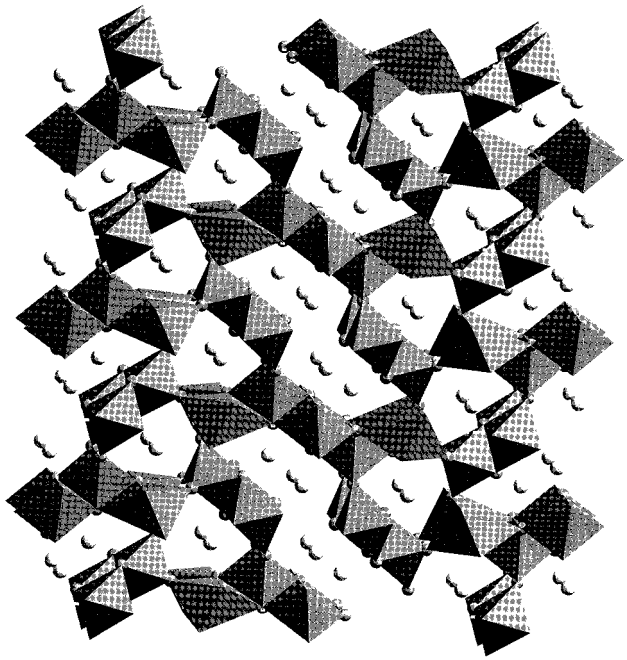

Figure 3. Structure of $Li_{0.44}MnO_2$.

B. Layered Structures. One of the most common manganese oxides with a layered structure is birnessite. There are three major variations of birnessite, turbostatic, single-layer hexagonal, and single-layer monoclinic structures. In general, birnessite structures have been poorly defined due to low crystallinity and small size of particles.

Recent XRD, selected-area electron diffraction (SAED), and extended X-ray absorption fine structure (EXAFS) studies have provided details about local structures,

substructures, superstructures, and the nature of defects in birnessite.[18,19] In such studies, Drits et al.[19] examined synthetic sodium birnessite and Sr^{2+} and H^+ derivatives by XRD and SAED. Sodium birnessite was found to consist of a layered monoclinic structure with subcell parameters of $a = 5.172$ Å, $b = 2.849$ Å, $c = 7.34$, and $\beta = 103.3°$. Very few vacancies were observed. Jahn−Teller distortions were attributed to Mn^{3+} substitution for Mn^{4+}. Superstructures in the *b* direction, namely, $B = 3b$, are caused by sodium ordering in the interlayer space. Based on these models, ideal structural formula are proposed: $Na_{0.33}(Mn_{0.722}Mn_{0.222}Mn_{0.05})O_2$ for NaBir I, and $Mn^{2+}_{0.833}Mn_{0.167}O_2$ for NaBir II.

The H^+ birnessite shows SAED diffraction patterns that are consistent with hexagonal cell parameters of $a = 2.84$ Å or base-centered cell parameters of $a = 4.927$, $b = 2.84$ Å and $\beta = 90°$. This pattern also shows weak additional reflections with a superlattice of $A = 3a$, $B = b$, and $\beta = 90°$. This suggests an ordered distribution of vacancies with associated interlayer $Mn^{2/3+}$ and H_2O molecules that are located above or below such vacancies.

The XRD and SAED studies of Ca^{2+}-exchanged birnessite reveal a four-layer monoclinic subcell structure with $a = 5.150$, $b = 2.844$, $c = 4c' = 28.16$ Å, and $\beta = 90.3°$. The superstructure arises from Mn^{3+} ordering within the layers and Ca^{2+} ordering between the layers, similar to that in sodium birnessite.[20]

C. EXAFS Studies. EXAFS spectroscopy has been used to study a variety of porous manganese oxide materials. The radial distribution functions (RDF) derived from EXAFS at Mn−K edges provide information about local manganese bonding environments. Using standard manganese oxides of known structure, such as pyrolusite, ramsdellite, and romanechite, RDF peaks at 1.6, 2.3−2.6, and 3.1 Å can be assigned to Mn−O, Mn−Mn (edge-sharing octahedra), and Mn−Mn (corner-sharing octahedra) interactions, respectively.[20] Manganese RDFs for H^+ birnessite are different from the Na^+ form and have a prominent peak at 3.1 Å, which corresponds to Mn−Mn distances in corner-shared MnO_6 octahedra. The intensities of these peaks vary for samples prepared at different pH values, but the general features are quite similar. The Mn RDFs for chalcophanite are almost identical to H^+ birnessite, indicating a similar structure for both materials. The quantitative analysis of numbers of edge- and corner-shared MnO_6 neighbors suggest that layer vacancies are restricted to every third row of Mn cations, with 50% of the Mn sites along these rows being vacant. This suggestion is consistent with SAED results.

D. Porosity. The porosity of microporous OMS-1 and OMS-2 materials has recently been published.[13b] These studies have clearly shown that broad pore size distributions are observed for these systems, as expected from the size and shape of the tunnels shown in Scheme 2. For example, OMS-1 has pore size distributions ranging from ∼6 to 9 Å, which is consistent with the largest distance across the diagonal sides of the tunnels of ∼9.6 Å. Such porosity is retained up to 650 °C. OMS-2 also has a wide pore size distribution, ranging from ∼4.5 to 7 Å. The layered material OL-1 has no such peak in the micropore pore size distribution. It is clear from such studies that the nature of the tunnel cations, framework cations, and specific structures markedly influence the pore size distributions.

The broad pore size distributions are quite different from zeolitic materials. One complication in the pore size distribution analysis is that a cylindrical pore model rather than a square pore model was used. Further studies and the development of a square pore model are underway. In addition, the adsorption capacity of these materials is on the order of 18−20 g of adsorbate per 100 g of adsorbent.[2] Such adsorption capacity rivals zeolitic type materials and has been recognized for natural manganese nodules.[1−13] The porosity of other materials already discussed were not reported, however, structural properties suggest that they should be porous.[15−20]

Transition Metal Oxide Mesoporous Materials

Mesoporous materials have been the focus of intense interest since the discovery of M41S materials by researchers at Mobil.[21] Most research in this area has involved aluminosilicate type materials with tetrahedral coordination. The formation of hexagonal mesoporous structures has been proposed to occur by a structural transformation of layers via heating or autoclave treatment of intercalated layered structures.[22] Recently, there have been considerable efforts in preparing transition metal oxide mesoporous materials. Ti-, Cr-, and V-substituted cubic MCM-48 mesoporous phases have been prepared by Pinnavaia et al.[23] Various transition metal (TM) sources, including chlorides and sulfates, were used to substitute the Si element in the framework of MCM-48 materials. The average pore size was ∼2.3 nm, with wall thicknesses of ∼0.5 nm. These TM-substituted MCM-48 materials were used to oxidize olefins. Vanadyl isopropoxide and sodium dioctyl sulfosuccinate surfactant were used to prepare vanadium oxide mesoporous materials.[24] A microemulsion was used to prepare nanoparticles of V_2O_5 with microporosity.

Ying et al. have made extensive contributions in making TM mesoporous materials, especially the recently reported niobium oxide and tantalum oxide mesoporous phases.[25−27] A novel ligand-assisted templating mechanism has been proposed for mesoporous niobium oxide.[25] A new amino(ethoxy)−niobium complex, formed from the reaction of niobium ethoxide and alkylamine, was treated with water followed by removal of surfactant by $EtOH/H_2O$ washing ($T \sim 40$ °C and pH = 1−2) to form crystalline hexagonal mesoporous phases. These materials are stable at 400 °C, and have a surface area of 400−600 m^2/g and a mesopore size of 2.7 nm.

Systematic studies of this niobium oxide system by Antonelli et al.[26] suggest a ligand-assisted liquid crystal templating mechanism. Starting conditions in syntheses, such as temperature, metal-to-surfactant ratio, pH, and solvent, are more important than aging time for the preparation of stable materials.

Tantalum oxide mesoporous materials with hexagonal structures have been reported by Antonelli and Ying.[27] Various chain-lengths of 12 to 18 carbons in surfactants have been used. To prepare materials with pore sizes varying from 2.2 to 4.0 nm, surface areas of ∼500 m^2/g, a hydrocarbon uptake of 0.23 g (1-butane)/g, and

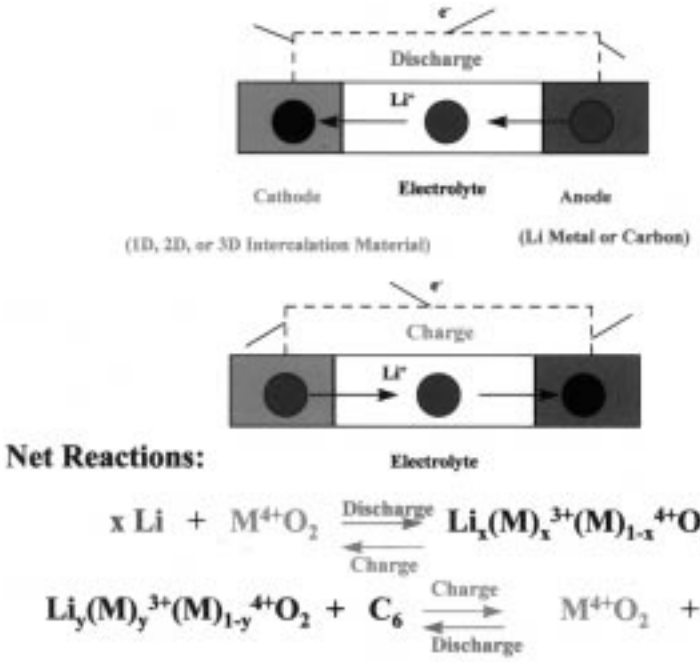

Figure 4. Charge and discharge mechanism and net reactions for lithium batteries (eq 1) and lithium ion batteries (eq 2).

thermal stability up to 450−500 °C. A controlled hydrolysis of long-chain primary amine complexes of $Ta(OEt)_5$ with a similar ligand-assisted templating mechanism was used.

A new family of manganese oxide structures (MOMS)[28] of both hexagonal and cubic phases have been prepared via incorporation of surfactant micelles and partial oxidation of $Mn(OH)_2$. Further oxidation of Mn^{2+} to Mn^{4+} and Mn^{3+} is accompanied by the removal of surfactants during calcination. The mesopore wall materials are believed to be microcrystallites of manganese oxides composed of primary building blocks of (MnO_6) octahedra.

These MOMS materials structures are thermally stable (up to 1000 °C), semiconducting (conductivity of $8.13 \times 10^{-6}\ \Omega^{-1}\ cm^{-1}$), and catalytically active (conversions of ∼10% and 8%, respectively, for catalytic oxidation of cyclohexane and *n*-hexane). Mesopores of 3.0 nm in diameter and 1.7 nm thick walls were observed for the hexagonal MOMS-1 phase.

Kuroda et al. have recently reported the syntheses of highly ordered mesoporous materials derived from Kanemite.[29] The synthesis could be divided into two steps: the exchange of interlayered Na^+ cations with alkylammonium cations at a pH of 11.5 and the condensation of silicates to form mesostructures at pH 8.5. These folded sheet mesoporous phases (FSM-16) can have high regularity and thermal stability. FSM-16 phases are stable up to 900 °C, and have surface areas of 900−1000 m^2/g and pore sizes of 1.5−3.2 nm.

Mesoporous manganese oxide materials have been reported to be transformed from layered birnessite,[30] using three approaches (oxidation, reduction, and layer transformation). In the oxidation process, O_2 was introduced into a mixture of $Mn(OH)_2$ and the surfactant oxidized Mn^{2+} to Mn^{3+} and Mn^{4+}. In the reduction process, alcohol was used to reduce trialkylammonium permanganate to form an amorphous manganese oxide mixed with surfactants. Aging this mixture leads to mesoporous materials. In the layer transformation approach, alkylammonium cations were used to exchange H^+ cations in H birnessite. The resulted mesophase is almost identical to what was formed by the oxidation method.

Electrochemical Studies of Porous Manganese Oxides

Manganese oxides are very important materials for applications in both aqueous and nonaqueous batteries (rechargeable and nonrechargeable). A few examples of the recent work in this wide field are described here.

A. Nonaqueous Systems. The search for high-energy density rechargeable batteries has led to significant developments of materials for different components of battery systems (anode, cathode, and electrolyte). In particular, attention has been focused on advanced lithium batteries with intercalation materials (open structure) as positive electrodes. Some of these are now commercially available, like the carbon/$LiCoO_2$ system (Sony Energytec Inc.)[31] and the carbon/ $LiNiO_2$ system (Moli Energy Ltd.).[32]

In general, chemical reactions that take place in an advanced lithium cell[33] consist of lithium ion intercalation (insertion) into the host lattice of the cathode during discharge (reduction), followed by deintercalation from the host lattice during recharging (oxidation), without significant modification of the host structure (reversible reaction). A schematic presentation is shown in Figure 4. using a metal oxide (MO_2) as an intercalation cathode.

Manganese oxides having good electrochemical performance are attractive as cathode materials for lithium cells because manganese has economic and environmental advantages over compounds based on cobalt or nickel. The largest part of electrochemical studies related to lithium intercalation in manganese oxides has been devoted to those materials with spinel-type phases, which are relatively nonporous materials.[34]

Materials having structures different than spinels have also been studied. Classical porous Na birnessite

and its ionic-exchanged compounds were investigated by Le Goff et al.[35] The lithium capacity (# Li/Mn) for Ca^{2+} and Zn^{2+} exchanged forms (hexagonal) was higher than that for Na^+ and Ag^+ exchanged forms (monoclinic). The Ca^{2+} and Zn^{2+} ions can act as pillaring species that minimize structural variations during the lithium insertion process.

Leroux and Nazar[36] have prepared several amorphous alkaline porous manganese dioxides with general formulas $A_zMnO_y{\cdot}nH_2O$ and $Li_xA_zMnO_y{\cdot}nH_2O$ (A = Na, K) at low temperatures. These materials were synthesized by reacting $AMnO_4$ materials with oxalic acid and using LiCl in the case of the lithiated compounds. Both lithiated and nonlithiated materials with A = K had higher Li capacities than when A = Na. The LiK materials with reversible capacities as high as 0.85 Li/Mn were obtained in molar ratios of 0.25 ($C_2H_2O_4$/Mn) and 10 (LiCl/Mn). In general, LiK-samples show good electrochemical performance at high cycling rates >2−4.5 V.

Pistoia and Antonini[37] carried out electrochemical potential spectroscopy tests on nonporous α-, β-, γ-MnO_2 (electrochemical MnO_2 and chemical MnO_2) and porous ramsdellite. They correlated electrochemical behavior to the rutile content and to the kinds of tunnels present in these materials. A fully lithiated ramsdellite, prepared by in situ lithiation, can be used as a cathode for 3 V Li cells with stable capacities.

Johnson et al.[38] reported a stabilized α-MnO_2 electrode for rechargeable 3 V lithium cells which is an α-MnO_2/ramsdellite composite with interconnected material. This stabilized α-MnO_2 electrode showed better stability to lithium insertion/extraction reactions than single-phase anhydrous α-MnO_2 or ramsdellite electrodes.

B. Aqueous Systems. The electrochemistry of MnO_2 electrodes in aqueous solution has been studied for many years because manganese oxides are the most common cathodic materials for dry cells. A global reaction for a complete discharge of MnO_2 in alkaline electrolyte[39] can be written as:

$$MnO_2 + 2H_2O + 2e^- \rightarrow Mn(OH)_2 + 2OH^- \quad (3)$$

Although eq 3 looks simple, the reduction process involves two complex steps and other products different than $Mn(OH)_2$ are possible. Andersen published an excellent review[40] that included a description of MnO_2 electrode behavior in alkaline, Leclanche (zinc−carbon), and zinc chloride environments. Discussions of MnO_2 structures, effects on battery activity, discharge mechanisms, chemistry of recharging MnO_2 in alkaline solution, and MnO_2 deposition technology were also reviewed.

In a series of systematic studies, Donne et al.[41−43] investigated redox processes in strong alkaline media of electrolytic manganese dioxide (EMD), birnessite, chemically modified EMD (Bi-EMD), and birnessite (Bi-birnnesite) electrodes. Constant-current intermittent discharge, slow-scan cyclic voltammetry, and detection of soluble and solid intermediates during the reduction step were used. Their results supported a two-step reduction mechanism with an initial homogeneous reduction involving reactions in solid solution followed by a heterogeneous reduction involving formation of soluble intermediates. Bi-doped manganese dioxides electrodes were rechargeable because of the presence of Bi ions. Rechargeability in alkaline cells made of porous bismuth birnessites is well known since the middle 1980s.[44−46] The presence of bismuth prevents the formation of the spinel Mn_3O_4 phase (poor electroactivity), which is the main cause of irreversibility[47] in the MnO_2/alkaline system. The formation of Mn_3O_4 results from reaction 4:[48]

$$Mn^{2+}\,(aq) + 2\,Mn^{3+}\,(aq) \rightarrow Mn_3O_4\,(s) \quad (4)$$

Bode et al.[49] and Yu[50] studied the rechargeability of Bi-doped MnO_2 samples produced by decomposition of $KMnO_4$ and $Bi(NO_3)_3$ mixtures in acid solution. Slow-scan cyclic voltammetry studies showed good rechargeability and the existence of complexes between Mn(X) (X = $^{2+}$, $^{3+}$, $^{4+}$) and Bi^{3+} as shown in eq 5:

$$m[Mn(X)]\,(aq) + [Bi^{3+}]\,(aq) \rightarrow ([Bi\text{-}Mn]\,(aq) \quad (5)$$

The presence of Bi^{3+} disturbs the formation of Mn_3O_4 from dissolved Mn^{2+} and Mn^{3+} and prevents the production of a large-size spinel lattice.

Electrochemical intercalation of birnessite has also been done in aqueous solutions. An electrochemical and a chemical step (ion-exchange) were proposed to explain the electro-intercalation process. It is not clear why Na^+ and K^+ intercalate to a greater extent than other alkali ions.[50b]

Catalysis with Manganese Oxides

One of the most important industrial applications of manganese oxides is oxidation catalysis. Manganese oxides in combination with other transition-metal elements serve as highly active thermally stable catalysts for oxidation of a variety of volatile organic compounds (VOC). These catalysts can operate at temperatures significantly lower than comparable noble metal-based catalysts.[51]

Recently studies with manganese oxides have focused on environmental reactions such as ozone decomposition, oxidation of organic pollutants, reduction of nitric oxide, and NO and NO_2 decomposition.[52−60] Some new manganese oxides catalysts for synthesis of organics have been reported.[51,52]

Ozone decomposition by MnO_2 supported on Al_2O_3 has been studied in a flow reactor by Oyama et al.[52] for removing ozone generated by photocopiers, laser printers, sterilizers, and aircraft. Data of Oyama et al.[52] suggest that MnO_2/Al_2O_3 is active for ozone decomposition at 313 K, and the rate of ozone decomposition depended only on [O_3]. Oyama et al.[52] also suggested that the mechanism of ozone decomposition involves formation of an ionic intermediate with partial superoxide or peroxide character. MnO_2 is a p-type oxide that would tend to stabilize anionic species. Most of the catalysts already described are relatively nonporous materials.

Catalytic oxidation reactions of organic pollutants into benign products such as CO_2 and H_2O can be photocatalyzed with amorphous manganese oxide (MO) materials. Photoassisted catalytic oxidation of organic pollutants, such as alcohols and halogenated hydrocar-

bons, have been carried out by Chen et al.[53] and Lin et al.[54] The AMO materials were prepared by the reaction of $KMnO_4$ and oxalic acid. Some transition metals cations, such as Cu^{2+}, Cr^{3+}, Ni^{2+}, and Zn^{2+}, can be incorporated into AMO materials during synthesis. These AMO materials have high photoactivity, mixed valent manganese oxidation states, high surface areas (200 m^2/g), microporous structures, and the ability to lose lattice oxygen and create lattice vacancies that may be important in photooxidation reactions.

Chen et al.[53] have shown that photoactive AMO systems can convert alcohols to ketones, such as acetone from 2-propanol, with 100% selectivity at room temperature; that AMO materials have turnover numbers that are over an order of magnitude greater than TiO_2 for decomposition of halogenated hydrocarbons, such as methyl bromide, to yield CO_2, H_2O, and Br_2; and that AMO is also active in the decomposition of CH_3Cl and CH_3I. In addition, Lin et al.[54] propose that methyl bromide degradation over AMO materials was due to a combination of photocatalytic and thermal reactions, but the photocatalytic reaction was predominant; and that oxygen sources for oxidation of methyl bromide might come from both molecular oxygen and bulk lattice oxygen from AMO materials.

Recent intensive studies on selective catalytic reduction (SCR) of nitric oxide with ammonia over MnO_2 (relatively nonporous)/Al_2O_3 were also reported by Bliek et al.[55−57] Compared with commercial catalysts based on V_2O_3/TiO_2, which require an operating temperature >575 K for SCR of nitric oxides, the two significant advantages of MnO_2/Al_2O_3 catalysts are the low operating temperature range (383−575 K) and nitrous oxide formation is almost absent up to 575 K.[55] Bliek et al.[55−57] have also investigated the mechanism of SCR of NO with ammonia over MnO_2/Al_2O_3 catalysts by using temperature-programmed desorption (TPD) and Fourier transform infrared (FTIR) methods. The mechanism of SCR of NO over these MnO_2/Al_2O_3 catalysts are closely related to the Lewis and Brönsted acid sites on the surface of the catalysts. The effects of the presence of O_2 and reaction temperature have also been reported in detail in these studies.[56,57]

Studies of NO and NO_2 decomposition over Mn_2O_3 and Mn_3O_4 have been quite intensively reported by Vannice et al.[58−60] In studies of decomposition of NO_2 over Mn_2O_3 and Mn_3O_4 catalysts, Vannice et al.[58] suggested that this reaction requires temperatures of >773 K for significant rates to occur. Mn_2O_3 is more active than Mn_3O_4 for NO decomposition, perhaps because Mn_2O_3 releases more lattice oxygen than Mn_3O_4 during reaction as observed by TPD studies.[60] The reaction pathway follows the Langmuir−Hinshelwood model involving a surface reaction between two NO molecules.[58] In studies of N_2O decomposition over manganese oxides, MnO, Mn_2O_3, Mn_3O_4, and MnO_2 are catalytically active for N_2O decomposition at 623 K, however, only Mn_3O_4 and Mn_2O_3 are stable. Mn_2O_3 is more active Mn_3O_4 catalysts.[59]

Menezo et al.[61] recently reported studies of the effects of chromium and manganese oxides on the structural and catalytic properties of copper/zirconia used for methanol synthesis from carbon dioxide and hydrogen.[61] Menezo et al.[61] suggest that addition of chromium and manganese oxides to copper/zirconia methanol synthesis catalysts results in increased thermal stability of the catalysts and no loss of activity. Menezo et al.[61] suggest that Mn or Cr suppressed sintering of the copper crystallites and stabilized the amorphous state of zirconia.

Ma et al.[62] recently reported catalytic and structural properties of manganese oxide supported on zirconia with mesoporous structures and high surface area. These manganese oxide catalysts were prepared by two different synthetic routes, grafting from an alkoxide precursor and conventional aqueous wet impregnation techniques. Samples prepared by grafting techniques allow manganese oxide to be highly dispersed and deposited on zirconia layers and result in multiple layers of manganese oxide with minor crystallinity on the support. This phenomena was not observed with the conventional impregnation technique. Differences in catalytic activity in CO oxidation, N_2O, and 2-propanol decomposition were observed. Strong interactions between manganese oxide and the support via grafting led to changes in properties of the manganese oxide from oxidizing to acidic.

Acknowledgment. We gratefully acknowledge the support of the U.S. Department of Energy, Office of Basic Energy Sciences, Division of Chemical Sciences for our research concerning porous manganese oxides. We thank J. M. Newsam of MSI for helpful discussions.

References

(1) Luo, J.; Suib, S. L. *J. Phys. Chem., B* **1997**, *101*, 10403−10413.
(2) Shen, Y. F.; Zerger, R. P.; DeGuzman, R.; Suib, S. L.; McCurdy, L.; Potter, D. I.; O'Young, C.-L. *Science* **1993**, *260*, 511−515.
(3) Feng, Q.; Sun, E.-H.; Yanagisawa, K.; Yamasaki, N. *J. Ceram. Soc. Jpn.* **1997**, *105*, 564−568.
(4) Feng, Q.; Yanagisawa, K.; Yamasaki, N. *J. Ceram. Soc. Jpn.* **1996**, *104*, 897−899.
(5) Feng, Q.; Yanagisawa, K.; Yamasaki, N. *Chem. Commun.* **1996**, 1607−1608.
(6) Rziha, T.; Gies, H.; Rius, J. *Eur. J. Mineral.* **1996**, *8*, 675−686.
(7) Witzemann, E. J. *J. Am. Chem. Soc.* **1915**, *37*, 1079−1091 and references therein.
(8) Bach, S.; Henry, M.; Baffier, N.; Livage, J. *J. Solid State Chem.* **1990**, *88*, 325−333.
(9) Ching, S.; Landrigan, J. A.; Jorgensen, M. L.; Duan, N.; Suib, S. L.; O'Young, C.-L. *Chem. Mater.* **1995**, *7*, 1604−1606.
(10) Duan, N.; Suib, S. L.; O'Young, C.-L. *J. Chem. Soc., Chem. Commun.* **1995**, 1367−1368.
(11) Ching, S.; Roark, J. L.; Duan, N.; Suib, S. L. *Chem. Mater.* **1997**, *9*, 750−754.
(12) Ching, S.; Petrovay, D. J.; Jorgensen, M. L.; Suib, S. L. *Inorg. Chem.* **1997**, *36*, 883−890.
(13) (a) Zhang, Q.; Luo, J.; Vileno, E.; Suib, S. L. *Chem. Mater.* **1997**, *9*, 2090−2095. (b) O'Young, C. L.; Sawicki, R. A.; Suib, S. L. *Microporous Mater.* **1997**, *11*, 1−8.
(14) Arafat, A.; Jansen, J. C.; Edaid, A. R.; Van Bekkum, H. *Zeolites* **1993**, *13*, 162−165.
(15) Boullay, P.; Hervieu, M.; Raveau, B. *J. Solid State Chem.* **1997**, *132*, 239−248.
(16) Rao, C. N. R.; Cheetham, A. K.; Mahesh, R. *Chem. Mater.* **1997**, *8*, 2421−2432.
(17) Armstrong, A. R.; Huang, H.; Jennings, R. A.; Bruce, P. G. *J. Mater. Chem.* **1997**, *8*, 255−259.
(18) Drits, V. A.; Silvester, E.; Gorshkov, A. I.; Manceau, A. *Am. Mineral.* **1997**, *82*, 946−961.
(19) Silvester, E.; Manceau, A.; Drits, V. A. *Am. Mineral.* **1997**, *82*, 962−978.
(20) Drits, V. A.; Lanson, B.; Gorshkov, A. I.; Manceau, A. *Am. Mineral.* **1998**, *83*, 97−118.
(21) Kresge, C. T.; Leonowicz, M. E.; Roth, W. J.; Vartuli, J. C.; Beck, J. S. *Nature* **1992**, *35*, 710−712.
(22) Yanagisawa, T.; Shimizu, T.; Kuroda, K.; Kato, C. *Bull. Chem. Soc. Jpn.* **1990**, *63*, 988−992.
(23) Zhang, W.; Pinnavaia, T. J. *Catalysis Lett.* **1996**, *28*, 261−265.
(24) Desai, S. D.; Cussler, E. L. *Langmuir* **1997**, *13*, 1496−1500.

(25) Antonelli, D. M.; Ying, J. Y. *Angew. Chem., Int. Ed. Eng.* **1996**, *35*, *4*, 426−430.
(26) Antonelli, D. M.; Nakahira, A.; Ying, J. Y. *Inorg. Chem.* **1996**, *35*, 3126−3136.
(27) Antonelli, D. M.; Ying, J. Y. *Chem. Mater.* **1996**, *8*, 874−881.
(28) Tian, Z. R.; Tong, W.; Wang, J. Y.; Duan, N. G.; Krishnam, V. V.; Suib, S. L. *Science* **1997**, *276*, 926−930.
(29) Inagaki, S.; Koiwai, A.; Suzuki, N.; Fukushima, Y.; Kuroda, K. *Bull. Chem. Soc. Jpn.* **1996**, *69*, 1449−1457.
(30) Luo, J.; Suib, S. L. *Chem Commun.* **1997**, 1031−1032.
(31) Nagaura, T. *4th International Rechargeable Battery Seminar*, Deerfield Beach, FL, 1990.
(32) Dahn, J. R.; Von Sacken, U.; Jukow, M. R.; Al-Janaby, H. *J. Electrochem. Soc.* **1991,** *138*, 2207−2211.
(33) Hossain, S. In *Handbook of Batteries*, 2nd ed.; Linden, D., Ed.; McGraw-Hill: New York; 1995; Chapter 36.
(34) Koksbang, R.; Barker, J.; Shi, H.; Saidi, M. Y. *Solid State Ionics* **1996**, *84*, 1−21.
(35) Le Goff, P.; Baffier, N.; Bach, S.; Pereira-Ramos, J. P. *Mater. Res. Bull.* **1996**, *31*, 63−75.
(36) Leroux, F.; Nazar, L. F. *Solid State Ionics* **1997**, *100*, 103−113.
(37) Pistoia, G.; Antonini, A. *J. Electrochem. Soc.* **1997**, *144*, 1553−1559.
(38) Johnson, C. S.; Mansuetto, M. F.; Thackeray, M. M.; Shao-Horn, Y.; Hackney, S. A. *J. Electrochem. Soc.* **1997**, *144*, 2279−2283.
(39) Liang, C. C. In *Encyclopedia of Electrochemistry of the Elements*, Vol. 1; Bard, A. J., Ed.; Marcel Dekker: New York; 1973; pp 349−403.
(40) Andersen, T. N. In *Modern Aspects of Electrochemistry*; White, R. E.; Conway, B. E.; Bockris, J. O'M., Eds.; Plenum: New York; 1996; pp 313−413.
(41) Donne, S. W.; Lawrance, G. A.; Swinkels, D. A. *J. Electrochem. Soc.* **1997**, *144*, 2949−2953.
(42) Donne, S. W.; Lawrance, G. A.; Swinkels, D. A. *J. Electrochem. Soc.* **1997**, *144*, 2954−2961.
(43) Donne, S. W.; Lawrance, G. A.; Swinkels, D. A. *J. Electrochem. Soc.* **1997**, *144*, 2961−2967.
(44) Yao, Y. F. U.S. Patent 4, 520, 005, May 28, 1985.
(45) Yao, Y. F.; Gupta, N.; Wroblowa, H. S. *J. Electroanal. Chem.* **1987**, *223*, 107−110.
(46) Wroblowa, H. S.; Gupta, N. *J. Electroanal. Chem.* **1987**, *238*, 93−102.
(47) Boden, D.; Venuto, C. J.; Wisler, D.; Wylie, R. B. *J. Electrochem. Soc.* **1968**, *115*, 333−338.
(48) Qu, D. Y.; Conway, B. E.; Bai, L.; Zhou, Y. H.; Adams, W. A. *J. Appl. Electrochem.* **1993**, *23*, 693−706.
(49) Bode, M.; Cachet, S.; Pereira-Ramos, J. P.; Ginoux, J. C.; Yu, L. T. *J. Electrochem. Soc.* **1997**, *144*, 792−801.
(50) (a) Yu, L. T. *J. Electrochem. Soc.* **1997**, *144*, 802−809. (b) Kanoh, H.; Tang, W.; Makita, Y.; Ooi, K. *Langmuir* **1997**, *13*, 6845−6849.
(51) *Kirk-Othmer Encyclopedia of Chemical Technology*, 4th ed.; Plenum Press: New York, 1991; Vol. 15, pp 1044−1045.
(52) Dhandapani, B.; Oyama, S. T. *Chem. Lett.* **1995**, 413−414.
(53) Chen, J.; Lin, J. C.; Purohit, V.; Cutlip, M. B.; Suib, S. L. *Catal. Today* **1997**, *33*, 205−214.
(54) Lin, J. C.; Chen, J.; Suib, S. L.; Cutlip, M. B.; Freihaut, J. D. *J. Catal.* **1996**, *161*, 659−666.
(55) Kijlstra, W. S.; Daamen, J. C. M. L.; Graaf, J. M. V. D.; Linden, B. V. D.; Poels, E. K.; Bliek, A. *Appl. Catal. B: Environ.* **1996**, *7*, 337−357.
(56) Kijlstra, W. S.; Brands, D. S.; Poels, E. K.; Bliek, A. *J. Catal.* **1997**, *171*, 208−218.
(57) Kijlstra, W. S.; Brands, D. S.; Smit, H. I.; Poels, E. K.; Bliek, A. *J. Catal.* **1997**, *171*, 219−230.
(58) Yamashita, T.; Vannice, M. A. *J. Catal.* **1996**, *161*, 254−262.
(59) Yamashita, T.; Vannice, M. A. *J. Catal.* **1996**, *163*, 158−168.
(60) Yamashita, T.; Vannice, M. A. *Appl. Catal. B: Environ.* **1997**, *13*, 141−155.
(61) Menezo, J. C.; Inkari, S.; Bertin, T.; Barbier, J.; Davias-Bainier, N.; Noirot, R.; Seguelong, T. *Appl. Catal. B: Environ.* **1998**, *15*, L1−L4.
(62) Ma, J.; Chuah, G. K.; Jaenicke, S.; Gopalakrishnan, R. Tan, K. L. *Ber. Bunsen.-Ges.* **1996**, *100*, *5*, 585−593.

CM980227H